Journal of Hazardous Materials 211–212 (2012) 104–111

Contents lists available at SciVerse ScienceDirect

Journal of Hazardous Materials

journal homepage: www.elsevier.com/locate/jhazmat

Ionothermal synthesis of hierarchical BiOBr microspheres for water treatment

Dieqing Zhang[a,b], Meicheng Wen[a], Bo Jiang[a], Guisheng Li[a], Jimmy C. Yu[b,*]

[a] The Education Ministry Key Lab of Resource Chemistry and Shanghai Key Laboratory of Rare Earth Functional Materials, Shanghai Normal University, 100 Guilin Road, Shanghai 200231, China

[b] Department of Chemistry and Institute of Environment, Energy and Sustainability, The Chinese University of Hong Kong, Shatin, New Territories, Hong Kong, China

ARTICLE INFO

Article history:
Received 20 June 2011
Received in revised form 20 October 2011
Accepted 24 October 2011
Available online 29 October 2011

Keywords:
Ionothermal
Bismuth oxybromide
Water treatment
Hierarchical
Microspheres

ABSTRACT

Bismuth oxybromide (BiOBr) micropsheres with hierarchical morphologies have been fabricated via an ionothermal synthesis route. Ionic liquid acts as a unique soft material capable of promoting nucleation and in situ growth of 3D hierarchical BiOBr mesocrystals without the help of surfactants. The as-prepared BiOBr nanomaterials can effectively remove heavy metal ions and organic dyes from wastewater. They can also kill *Micrococcus lylae*, a Gram positive bacterium, in water under fluorescent light irradiation. Their high adaptability in water treatment may be ascribed to their hierarchical structure, allowing them high surface to volume ratio, facile species transportation and excellent light-harvesting ability.

1. Introduction

Bismuth oxyhalides are V–VI–VII ternary compounds with tetragonal crystal structure. They are layered structures that consist of a halide ion layer and a metal–oxygen layer. Their high stability against photocorrosion is advantageous for applications in photocatalysis and photoelectrochemical cells [1–3]. Several synthesis methods for mico- and nanostructures of BiOX materials have been reported in the literature. The size controllable synthesis of spherical BiOX nanoparticles with diameters of 3–22 nm was developed by Henle et al. using an effective reverse microemulsions route [4]. Deng et al. reported the synthesis of one-dimensional (1D) bismuth oxyhalide nanowires and nanotubes using a cationic surfactant cetyltrimethylammonium bromide (CTAB) as the bromine source [5]. Geng et al. described a procedure for one-step selective synthesis of two-dimensional (2D) BiOCl lamellae materials via a sonochemical method [6]. 2D single-crystalline BiOX (X = Cl, Br) nanoplates, nanosheets, and microsheets were obtained by hydrogen peroxide oxidation of bulk metal Bi particles in a surfactant-mediated solution [7]. Fabrication of three-dimensional (3D) BiOBr materials is more complicated. This may be achieved by using bismuth nitrate and inorganic halide salts as starting materials through a coprecipitation process [1,8]. It is still a big challenge to develop simple and reliable synthetic routes for hierarchically self-assembled bismuth oxyhalides architectures with specific morphologies.

Ionic liquids (ILs) are non-volatile and non-flammable organic salts with low melting points. The use of ILs is well documented in important fields such as synthetic–organic chemistry, separation and electrochemistry [9–11]. The value of ILs in the field of inorganic nanosynthesis has gradually been realized. In 2000, Dai's group first reported the synthesis of SiO_2 aerogel using an ionic liquid, 1-ethyl-3-methylimidazolium bis(trifluoromethylsulfonyl)imide ([EMim][NTf_2]), instead of water as the solvent [12]. Among the main advantages of using ILs as solvents or additives in inorganic synthesis is their superior capability for the solvation and stabilization of metal cations. This is why ILs are often used as capping agents or surfactants. These properties have been exploited to prepare nanoparticles of different compositions including pure metals [13–18], metal oxides [19–22], metal chalcogenides [23,24], silicas and organosilicas [25–29], metal salts [30–34], and carbon material [35,36]. Recently, our group reported an ionic-liquid based route for exposing the {0 0 1} reactive facets of anatase TiO_2 single crystals. The as-prepared photocatalysts show very high efficiency in decomposing organic pollutants [37,38]. Nevertheless, the full potential of ILs as the reagents in the controllable synthesis of inorganic nanostructures remains to be further explored.

Herein, we report that ionic liquid can act as a unique soft material capable of promoting the nucleation and in situ growth of 3D hierarchical bismuth oxybromide mesocrystals without using any surfactants. Our strategy for preparing BiOBr is based on the solvothermal reaction involving bismuth nitrate and an

* Corresponding author. Tel.: +852 3943 6268; fax: +852 2603 5057.
E-mail address: jimyu@cuhk.edu.hk (J.C. Yu).

0304-3894/$ – see front matter © 2011 Elsevier B.V. All rights reserved.
doi:10.1016/j.jhazmat.2011.10.064

imidazolium-based ionic liquid in triethylene glycol. The key in this method is the use of the 1-butyl-3-methyl-imidazolium IL which forms an ionic-liquid–bismuth complex which evolves into the final 3D superstructure. Ionic liquids are often considered "designer solvents" due to the unique variability of the ions. By selecting an appropriate anion for the ionic liquid, bismuth oxybromide can be synthesized. The chemical structure of the ionic liquid used in this work is shown below.

The as-prepared BiOBr products own 3D hierarchical structure with high surface to bulk ratio and facile species transportation. Such 3D hierarchical architectures allow the BiOBr materials to be utilized as strong adsorbent for waste-water treatment. They exhibited an excellent performance to remove heavy metals (Cr (VI)) and organic dyes (methylene blue). Interestingly, the photocatalysis-induced anti-bacteria properties of the 3D BiOBr microspheres were also investigated by using *Micrococcus lylae* as a model bacterium. They exhibited a unique ability in killing bacteria in water under fluorescent light irradiation.

2. Experimental

2.1. Sample preparation

In a typical synthesis of BiOBr hierarchical microspheres, 0.485 g of bismuth nitrate pentahydrate (ACROS) was dissolved in 10 mL of triethylene glycol (Panreac) in an ultrasonic bath. Then ionic liquid, 0.5 mL of 1-butyl-3-methyl-imidazolium-bromide (IL) was added into it under stirring. Then the mixture was put into a 50 mL Teflon-lined stainless autoclave. The autoclave was heated to 200 °C and maintained for 24 h. The resulting precipitates were collected and washed with ethanol and deionised water thoroughly and dried at 80 °C in air.

In a typical systhesis of BiOBr nanosheets, 0.485 g bismuth nitrate pentahydrate (ACROS) was dissolved in 10 mL benzyl alcohol under ultrasonic condition. Then 0.103 g sodium bromide was added into the above system. Then the mixture was put into a 50 mL Teflon-lined stainless autoclave. The autoclave was heated to 200 °C and maintained for 24 h. The resulting precipitates were collected and washed with ethanol and deionised water thoroughly and dried at 80 °C in air.

2.2. Characterization

The products were characterized by X-ray diffraction measurements which was carried out in a parallel mode (ω = 0.5°, 2θ varied from 20° to 80°) using a Bruker D8 Advance X-ray diffractometer (Cu Kα radiation, λ = 1.5406 Å). The morphology and the microstructures of the products were investigated by transmission electron microscope (TEM) and selected area electron diffraction (SAED) with a JEM-200CX (JEOL, 200 kV) TEM, and a high-resolution transmission electron microscope (HRTEM, JEOL-2010). The electron microscopy samples were recorded prepared by grinding and dispersing the powder in acetone with ultrasonication for 20 s. Carbon-coated copper grids were used as sample holders. The scanning electron microscopy images were recorded on an FEI Quanta 400 FEG microscope. The photoluminescent (PL) spectra were recorded on a Varian Cary-Eclipse 500. The diffuse reflectance spectra of the samples over a range of 200–800 nm were recorded by a Varian Cary 100 Scan UV-vis system equipped with a Labsphere diffuse reflectance accessory.

2.3. MB and Cr (VI) adsorption

Firstly, aqueous solutions containing different concentrations of MB (20–500 mg/L) and Cr (VI) (5–40 mg/L) were prepared. In this case, $K_2Cr_2O_7$ was used as the source of Cr (VI). All adsorption experiments were carried out at room temperature in an oscillator without stirring. For the adsorption rate tests for MB, 50 mg BiOBr adsorbents were added to 20 mL of MB (320 mg/L) solution and 70 mg BiOBr adsorbents were added to 50 mL Cr (VI) (37 mg/L) solutions. After adsorption process, solid and liquid were separated by centrifugation of the resulting suspension to measure the concentrations of MB and Cr (VI) in the solution. For adsorption isotherm studies, the 20 mL of MB and 50 mL of Cr (VI) solution with different concentrations were mixed with 50 and 70 mg BiOBr adsorbents for 3180 min and 360 min, respectively. The measurements of MB and Cr (VI) concentrations were carried out using a UV-7502 PC spectrophotometer. The MB concentration was determined by measuring the solution absorbance at 665 nm. The Cr (VI) concentration was spectrophotometrically determined at 353 nm using a Beer's law plot constructed from standard solutions [39,40]. A UV–visible spectrum of a Cr (VI) aqueous solution is shown in Supporting information Fig. S1. Under our experimental conditions, the absorption maximum was at 353 nm. This was agreement with the previous report [39,40]. Furthermore, we found good linear working range over Cr (VI) concentration of 5–40 mg/L as shown in Supporting information Fig. S2. The detection limit was estimated to be 2 mg/L. For reference, the BiOBr nanosheets were selected to compare the adsorption capacity to that of the hierarchical BiOBr microspheres.

2.4. Measurements of bactericidal activity

Micrococcus lylae, a Gram positive bacterium, was used as a model bacterium in the experiment. It was incubated in 10% trypticase soy broth (TSB) at 30 °C and agitated at 200 rpm for 24 h. The culture was washed with 0.9% saline by centrifugation at 21,000 rpm for 5 min at 25 °C and the pellet was resuspended in saline. The cell suspension was adjusted in centrifuged tube to the required cell concentration (1–2 × 10^8 cfu mL^{-1}). The photocatalyst BiOBr was added to 0.9% saline in a conical flask and homogenized by sonication. The suspension was then sterilized by autoclaving at 121 °C for 20 min, allowed to cool, and mixed with the prepared cell suspension. The final photocatalyst concentration was adjusted to 100 mg/L and the final bacterial cell concentration was 1–2 × 10^7 cfu mL^{-1}. The photocatalytic reaction was started by irradiating the mixture with fluorescent light and stopped by switching off the light. The light source used was four 15 W fluorescent lamps mounted closely on the top of the flask. The reaction mixture was stirred with a magnetic stirrer to prevent settling of the photocatalyst. Before and during the light irradiation, an aliquot of the reaction mixture was immediately diluted with 0.9% saline and plated on TSB agar. The colonies were counted after incubation at 37 °C for 48 h. The inactivation of bacterial population during PCO was calculated by the equation:

$$\text{Bacterial inactivation}\,(\%) = \frac{P_I - P_T}{P_I} \times 100$$

where P_I represented the initial population and P_T represented the population after irradiation time (T).

3. Results and discussion

3.1. XRD

X-ray diffraction (XRD) was used to characterize the phase structure and crystalline size of the sample. Fig. 1 shows the XRD patterns

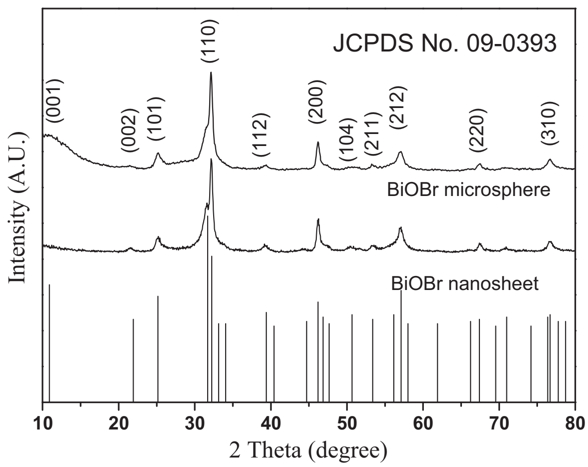

Fig. 1. XRD pattern of the as-prepared BiOBr samples.

of the as-prepared samples. Quantitative analysis of these pattern show that all peaks in the pattern can be assigned to the diffraction of (0 0 1), (0 0 2), (1 0 1), (1 1 0), (1 1 2), (2 0 0), (1 0 4), (2 1 1), (2 1 2), (2 2 0) and (3 1 0) planes of tetragonal bismuth oxide bromide (JCPDS card no. 09-0393, $a = 3.926$ Å and $c = 8.103$ Å), indicating the formation of BiOBr. The broad diffraction peaks suggest that the crystallite sizes of the BiOBr microsphere sample are small and the corresponding crystallite size, calculated by Scherrer formula, is 8.5 nm. As calculated, the BiOBr nanosheets have the same tetragonal phase structure and crystalline size.

3.2. SEM and TEM

Fig. 2a–d shows the field-emission scanning electron microscopy (FESEM) images of the ternary BiOBr powders with different magnifications. The samples were obtained under the solvothermal condition at 200 °C for 24 h. The low-magnification FESEM images (Fig. 2a and b) show the high-yield synthesis of mesocrystals with an average diameter of 4.5 μm. The particles are uniformly dispersed without obvious aggregation. The high yield of BiOBr is partly due to the hydrophilic characteristics and high dielectric constant ($\varepsilon = 11.7$) of the ionic liquid which can well support the dissolution of bismuth nitrate [41], facilitating the nucleation of crystal growth and promote the formation of crystalline products. This solution-based approach should be easily extended to large-scale production of BiOBr mesocrystals. Close inspection (Fig. 2c and d) shows an interesting 3D marigold-like morphology. The flower-like superstructures are composed of nanosheets with thickness of 15 nm, forming an open porous structure. It is quite probable that imidazolium-based ILs form a complex with bismuth at an early stage of the reaction. The assumption is based on the mesocrystal transformation features in recent reports [42–45]. They indicate that primary nanoparticles are the building units that assemble into larger structures, forming mesocrystals by oriented attachment and fusion. We believe that the ILs distributed over the nanosheets surface play an important role in the determination of inter-nanosheet interaction leading a 3D assembly process to reduce the surface energy and transforming into a marigold-like 3D structure. It is well known that ionic liquid solutions can be considered as a system of near-spherical charged micelles. At the beginning of the reaction, large amounts of nuclei of BiOBr were formed on the surface of the ionic liquid micelles. Then these BiOBr nuclei grew and transformed into nanosheets. Small nanosheets would aggregate on the surface, and then self-assembled into the hierarchical BiOBr structures. Our results are consistent with the previous

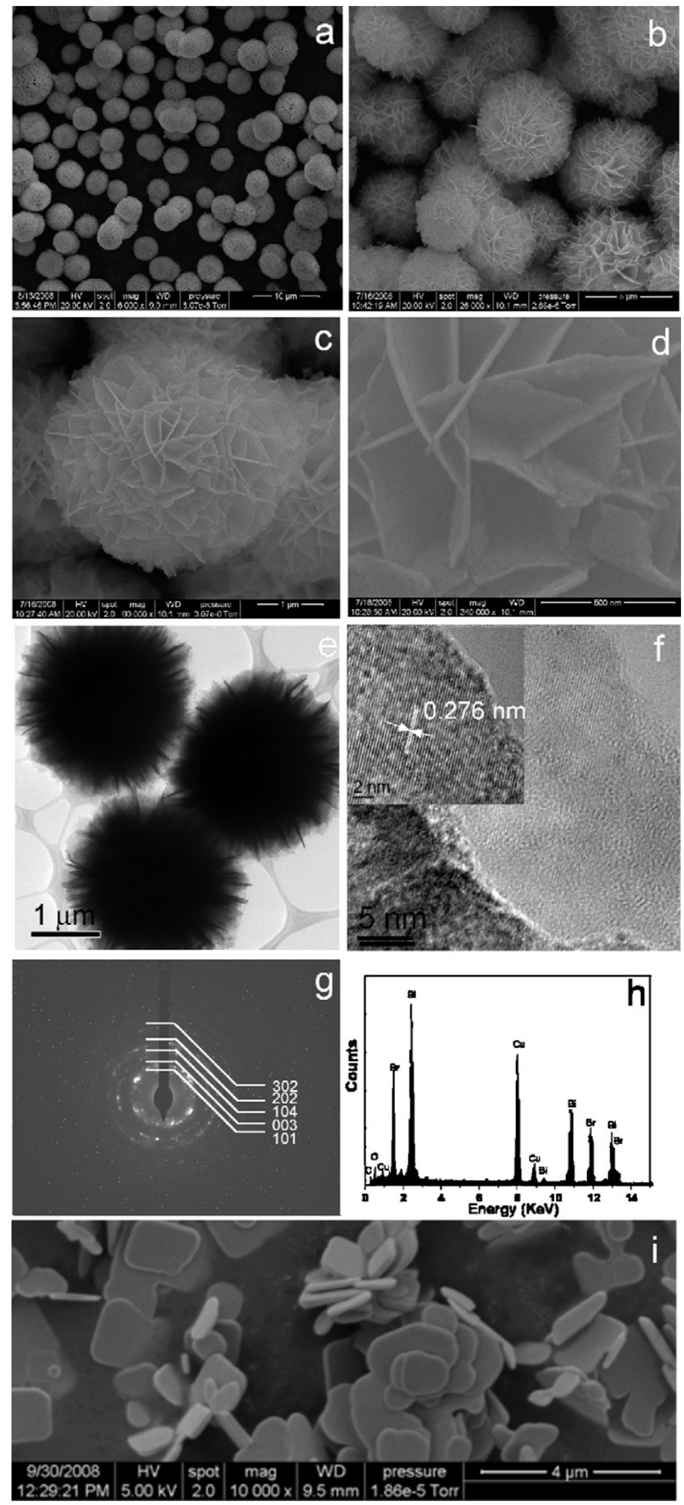

Fig. 2. FESEM images (a–d), TEM (e) and HRTEM (f) images, SAED (g) and EDX pattern (h) of BiOBr microspheres; FESEM image of the as-prepared BiOBr nanosheets (i).

work, where 1-butyl-3-methyl-imidazolium bromide (or chloride) supports three-dimensional alignment of silver nanoparticles [45]. The results of transmission electron microscopy (TEM) images give more detailed information regarding the interior structure of the flower-like architectures. Fig. 2e reveals that the entire structure is composed of several dozens of nanosheets with smooth surface. As shown in Fig. 2f, clear lattice fringes can be observed and the

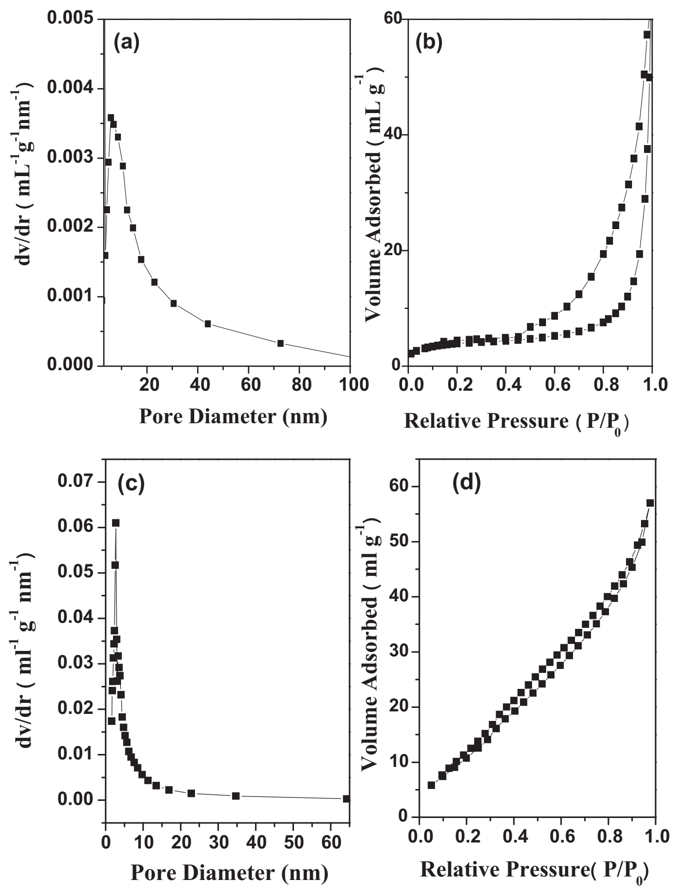

Fig. 3. Pore-size distributions and N_2 adsorption and desorption isotherms for the hierarchical BiOBr microspheres (a and b) and for the BiOBr nanosheets (c and d).

single crystalline nature of the nanosheet is revealed. The lattice spacing is about 0.276 nm as shown in the inset of Fig. 2f, which is consistent with the d-spacing of the (1 1 0) reflection for BiOBr. The selected area electron diffraction (SAED) analysis (Fig. 2g) confirms the high polycrystalline nature of BiOBr. Results of the energy dispersive X-ray (EDX) analysis (Fig. 2h) show the molar ratio of Bi:Br to be 1.1:1. Carbon and copper are from the conducting tape and the sample holder. We also fabricated BiOBr nanosheets for comparison. As shown in Fig. 2i, the as-prepared BiOBr nanosheets are dispersed with a size ranging from 1 to 2 μm and an average thickness of about 100 nm.

3.3. Specific surface areas and porosity

The specific surface area and porosity of the marigold-like BiOBr microspheres were measured from the nitrogen adsorption analysis. Fig. 3 presents the corresponding pore-size distribution curves (a) and the N_2 adsorption–desorption isotherms (b) for the hierarchical BiOBr sample. The samples exhibit type-IV isotherms (Fig. 3b) which is typical for mesoporous solids. The hysteresis loop in the relative pressure range between 0.4 and 0.9 is probably related to the pores present within nanopsheets, which are formed between primary crystallites. The high-pressure parts of the hysteresis loop ($0.9 < P/P_0 < 1$) are probably associated with textural larger pores that can be formed between secondary particles due to aggregation of nanoflakes into the flower-like superstructures. The pore diameters are estimated by using the desorption branch of the isotherm. The pore-size distribution curves are quite broad due to the presence of small and larger mesopores. The smaller mesopores reflects porosity in nanosheets, while larger mesopores can be related to the pores formed between stacked nanosheets [46]. The macroporous structure (ca. 100–500 nm) can be directly observed on the SEM images of the BiOBr sample shown in Fig. 2, which cannot be accessed by N_2 adsorption–desorption analysis. The BET specific surface area of the BiOBr sample calculated by the Brunauer–Emmett–Teller (BET) method is 14 m^2/g. Such a 3D marigold-like hierarchical macroporous framework is beneficial to enhance the adsorption efficiency of adsorbate molecules and their flow rates [47]. Therefore, the 3D BiOBr microsphere with micro- and nano-structures can be a promising candidate for various applications in the field of environmental remediation.

3.4. Cr (VI) removal

Chromium (VI) is a hazardous pollutant, and its efficient removal from the environment is of great importance. Fig. 4a shows a decrease of Cr (VI) concentration when 70 mg of the as-obtained hierarchical BiOBr microspheres was added to 50 mL Cr (VI) (37 mg/L) solution at room temperature. For comparison, we also investigated the adsorption rate of the BiOBr nanosheets under the same experimental conditions. It is clear from Fig. 4a that the adsorption rate of hierarchical BiOBr microspheres is two times fast than that of the BiOBr nanosheets. The Cr (VI) removal efficiency is concentration dependent. At a low concentration of 6.4 mg/L, 90% of Cr (VI) could be removed after 6 h. The fast Cr (VI) uptake indicates a high complexation rate between the pollutants and adsorbent, which is related to their primary crystallite size of adsorbents and unique hierarchical structure. The adsorption isotherms of Cr (VI) by the as-prepared BiOBr microspheres at different initial concentrations are illustrated in Fig. 4b. It reveals that the mass of adsorption increased with the increase of the initial concentration. The maximum adsorption capacity (q_m) was found to be 7.7 mg g^{-1} for hierarchical BiOBr microspheres. It was also found that the removal capacity of the as-obtained BiOBr nanosheets was only 4.0 mg g^{-1} for Cr (VI). Obviously, the as-prepared BiOBr microspheres with 3D micro- and nano-structures show much better removal capacity than that of the BiOBr nanosheets, even though the latter has a surface area (45 m^2/g), much higher than that of the former (14 m^2/g).

The BET results (Fig. 3c) show that the BiOBr nanosheets own a narrow pore size distribution at about 2.5 nm. Nevertheless, the BiOBr microspheres have a broad pore size distribution ranging from 4.0 nm to 25 nm. Thus, it is reasonable that such good performance for heavy metal removal by BiOBr microspheres could be attributed to the hierarchical macro/nanoporous structure. Adsorption systems have been always investigated by various adsorption models. Langmuir and Freundlich adsorption models have been proven as a useful model for many adsorption cases. In this work, the two models were utilized to analyze the Cr (VI) ions adsorption. The Langmuir adsorption model is used to represent the relationship between the amount of heavy metal adsorbed at equilibrium (q_e, mg g^{-1}) and the equilibrium solute concentration (C_e, mg/L):

$q_e = \frac{q_m b C_e}{1+bC_e}$ where q_m (mg g^{-1}) is the maximum sorption capacity corresponding to complete monolayer coverage and b is the equilibrium constant (L mg^{-1}).

When such a model was adopted to analyze the adsorption isotherms, good linear relations are obtained for Cr (VI) ions adsorption, indicating the experimental data fit well with Langmuir adsorption model as shown in Fig. 5. The correlation coefficient (R^2) was 0.9994 for Langmuir adsorption isotherm. This implies that the adsorbed layer is monolayer coverage. Cr (VI) is adsorbed on the BiOBr surface via the electrostatic attraction between the surface hydroxyl groups of BiOBr and CrO_4^{2-}. Thus, the homogeneous nature of surface hydroxyl groups led to Langmuir type adsorption.

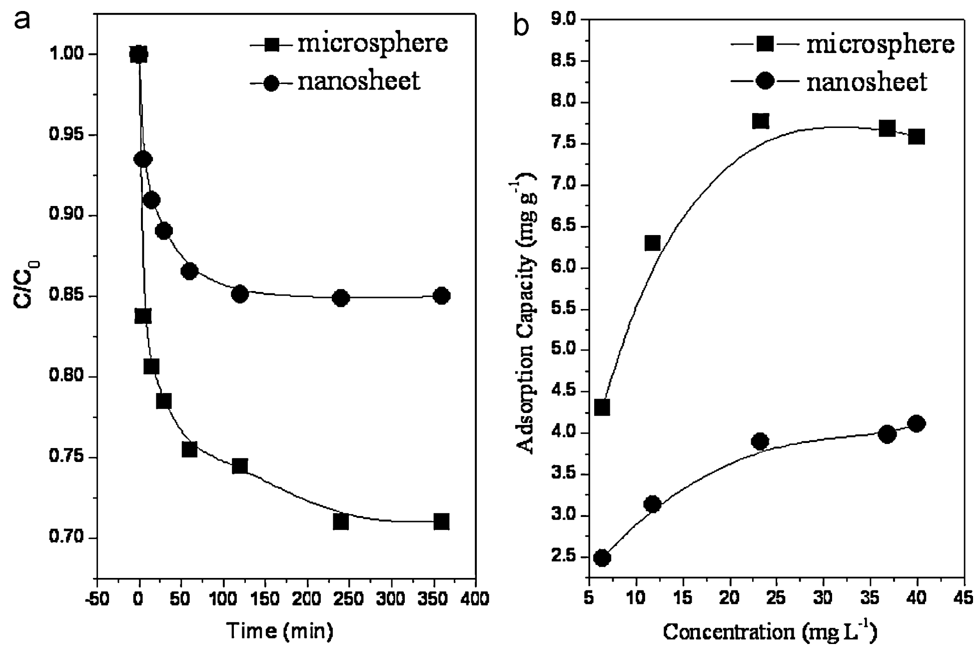

Fig. 4. (a) Adsorption rate of Cr (VI) on the hierarchical BiOBr microspheres (■) and BiOBr nanosheets (●). (b) Adsorption isotherms of Cr (VI) on the hierarchical BiOBr microspheres (■) and BiOBr nanosheets (●).

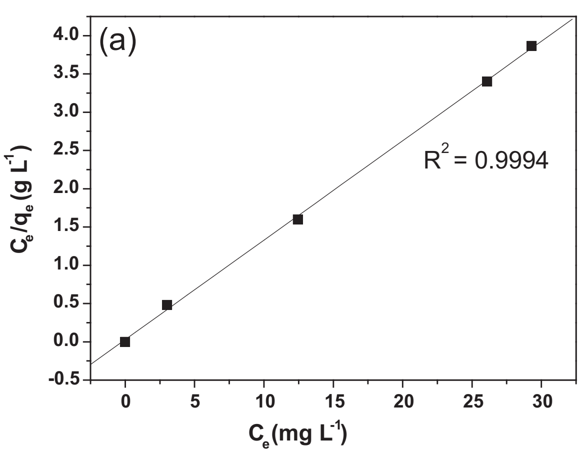

Fig. 5. Langmuir plot for Cr (VI) adsorption on the hierarchical BiOBr microspheres.

3.5. MB removal

The hierarchical BiOBr microspheres could also be used as adsorbents to remove organic waste from water by adsorption. Herein, a hazardous heterocyclic aromatic chemical compound, methylene blue (MB), was chosen as a typical organic waste. We used 50 mg of hierarchical BiOBr microsphere sample to treat 20 mL MB aqueous solution at 25 °C. When the initial concentration of MB in solution was as high as 320 mg/L, the hierarchical BiOBr microspheres could remove 55% of MB from the aqueous solution (shown in Fig. 6a). For comparison, we also investigated the adsorption rate of the BiOBr nanosheets under the same experimental conditions. Results show that the BiOBr nanosheets was much worse than the microspheres for MB adsorption (Fig. 6a). The adsorption isotherms of MB by the as-prepared BiOBr microspheres at different initial concentrations are illustrated in Fig. 6b. It reveals that the mass of adsorption increased with the increase of the initial concentration. The maximum adsorption capacity of the hierarchical BiOBr microspheres was found to be 75 mg g^{-1}, about 4 times of that of the BiOBr nanosheets (18 mg g^{-1}). Such greatly enhanced methylene blue adsorption capacity for 3D BiOBr microspheres may be ascribed to their hierarchical 3D microstructures. After immersing in Cr (VI) and MB solutions for 24 h, the crystal structure of BiOBr was still well maintained as shown in the XRD pattern (Supporting information Fig. S4). This suggests high stability for BiOBr.

3.6. Bactericidal activity

The BiOBr microspheres can not only act as an efficient adsorbent for toxic heavy metals and organic dyes but is also a good photocatalyst for the deactivation of pathogens. The bactericidal activity of the BiOBr sample was evaluated by killing *M. lylae* in water under fluorescent light (commonly used for householding lighting, visible light intensity = 7.48 mW/cm^2) irradiation on the basis of the decrease in the colony number of *M. lylae* formed on an agar plate. The fluorescent light photocatalytic disinfection is safe and cost effective as compared to disinfection using UV and chlorine since the latter ones use hazardous irradiation and produce disinfection by-products in the process [48]. The BiOBr microspheres in the dark show no bactericidal effects on *M. lylae*, indicating that the photocatalyst itself is not toxic to *M. lylae*.

As shown in Fig. 7, 50% of *M. lylae* were killed in 180 min and only 10% of *M. lylae* could survive after 360 min of light irradiation. It is known that oxygen species, such as hydroxyl radicals, formed within the BiOBr photocatalytic system can oxidize the cell membrane and destroy the microbial structure, causing various damages to living organism [49,50]. In order to confirm the presence of hydroxyl radicals, terephthalic acid (TA) was used as a fluorescence probe. Supporting information Fig. S3 displays the fluorescence spectra of the visible light irradiated BiOBr in 5 mM terephthalic acid and 0.01 M NaOH solution at different irradiation times. The unique fluorescence peak at 426 nm is observed, which is originated from 2-hydroxyterephthalic (TAOH) acid produced by the reaction of TA with hydroxyl radicals in basic solution under visible light irradiation. Such high photocatalytic bactericidal activity of BiOBr microspheres may be due to their strong adsorption capability, allowing a good ability to adhere to the cell

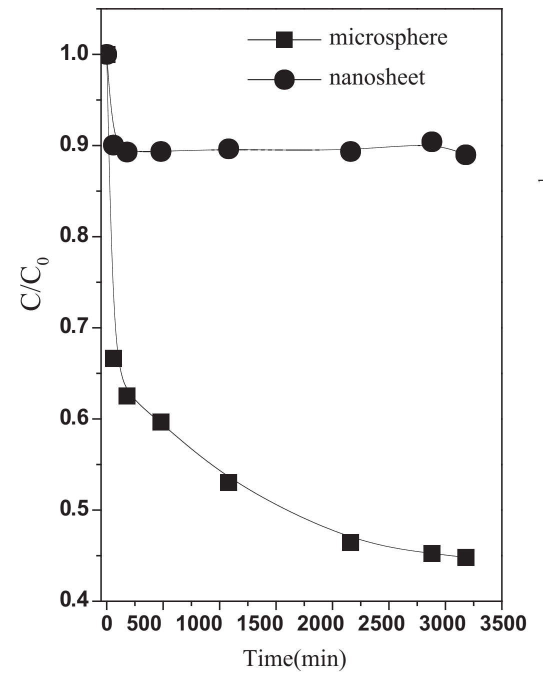

Fig. 6. (a) Adsorption rate of MB on the hierarchical BiOBr microspheres (■) and BiOBr nanosheets (●). (b) Adsorption isotherms of MB on the hierarchical BiOBr microspheres (■) and BiOBr nanosheets (●).

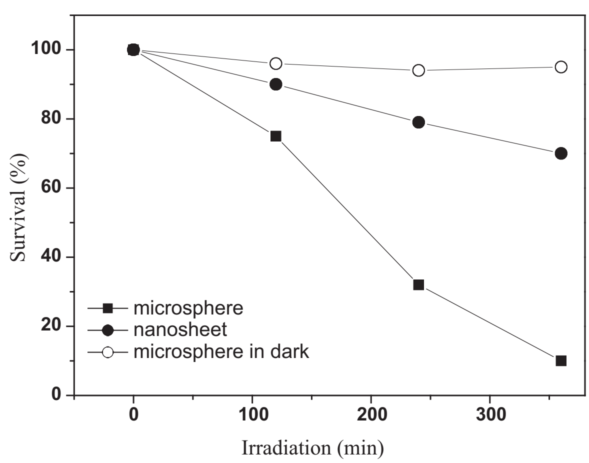

Fig. 7. Survival ratio of *M. lylae* vs irradiation time for BiOBr microspheres and BiOBr nanosheets.

membrane of *M. lylae*. The photocatalytic quantum efficiency of the BiOBr is another key factor responsible for its excellent bactericidal activity. As shown in Fig. 8a, the as-prepared BiOBr microspheres exhibited much higher light absorption intensity than the BiOBr nanosheets. This is because the hierarchical structures of the BiOBr microspheres may allow the light to multi-reflect between the BiOBr layers, thus, more light could be utilized to activate BiOBr crystals to generate electron–hole pairs with enhanced quantum efficiency for the photocatalytic oxidation of *M. lylae*. Such high quantum efficiency can be further proved by the PL results, which can allow one to investigate the recombination and lifespan of photogenerated electrons/holes in the photocatalysts. Fig. 8b shows the emission intensity at 390 nm of the BiOBr microspheres is much lower than that of the BiOBr nanosheets, indicating a lower recombination rate of photo-generated electrons and holes in the BiOBr microspheres [51]. Therefore, it is reasonable that much higher quantum efficiencies could be obtained on the microspheres for the photocatalytic reaction owing to the hierarchical structures of BiOBr microspheres.

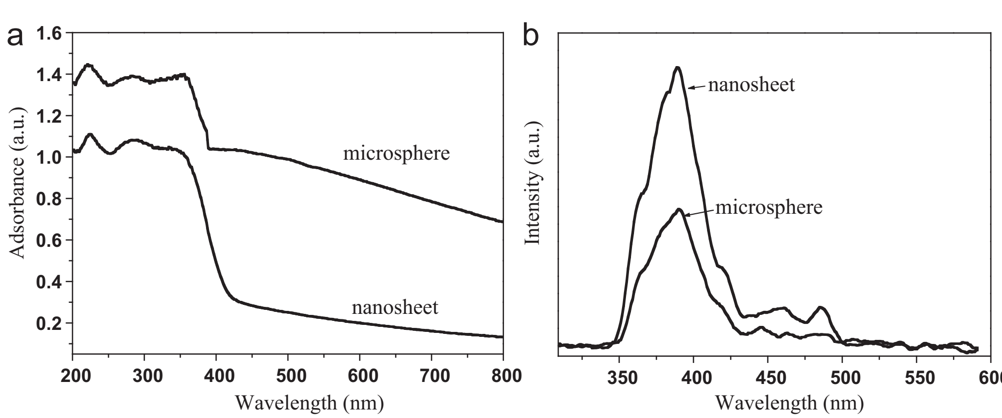

Fig. 8. UV–vis spectra (a) and PL spectra (b) of the as-obtained BiOBr microspheres and nanosheets.

4. Conclusion

In conclusion, 3D marigold-like BiOBr microspheres with high adaptability in water treatment were fabricated with imidazolium-based ionic liquids as a structural directing agent and the resource of bromine ions. The resulting BiOBr microspheres show high adsorption efficiency for heavy metals and organic dyes. The material can also be used as a photocatalyst for inactivating bacteria. This facile method may allow us to produce other metal halide plasmonic photocatalysts with 3D architectures, such as Ag/AgBr and Ag/AgCl.

Acknowledgements

We would like to thank supports from the Research Grants Council of Hong Kong (General Research Fund CUHK404810), the Program for Professor of Special Appointment (Eastern Scholar) at Shanghai Institutions of Higher Learning, the National Natural Science Foundation of China (21007040, 21047009), Natural Science Foundation of Shanghai Committee of Science and Technology (11ZR1426300), the Research Fund for the Doctoral Program of Higher Education (20103127120005), the Project supported by the Shanghai Committee of Science and Technology (10160503200), the Project supported by Innovation Program of Shanghai Municipal Education Commission (12YZ079) and by a Scheme administrated by Shanghai Normal University (SK201104). We also thank Prof. P. K. Wang's group (Department of Biology of The Chinese University of Hong Kong) for their assistance on the measurements of bactericidal activity.

Appendix A. Supplementary data

Supplementary data associated with this article can be found, in the online version, at doi:10.1016/j.jhazmat.2011.10.064.

References

[1] J. Zhang, F.J. Shi, J. Lin, D.F. Chen, J.M. Gao, Z.X. Huang, X.X. Ding, C.C. Tang, Self-assembled 3-D architectures of BiOBr as a visible light-driven photocatalyst, Chem. Mater. 20 (2008) 2937–2941.
[2] K.L. Zhang, C.M. Liu, F.Q. Huang, C. Zheng, W.D. Wang, Study of the electronic structure and photocatalytic activity of the BiOCl photocatalyst, Appl. Catal. B 68 (2006) 125–129.
[3] S.K. Poznyak, A.I. Kulak, Photoelectrochemical properties of bismuth oxyhalide flims, Electrochim. Acta 35 (1990) 1941–1947.
[4] J. Henle, P. Simon, A. Frenzel, S. Scholz, S. Kaskel, Nanosized BiOX (X = Cl, Br, I) particles synthesized in reverse microemulsions, Chem. Mater. 19 (2007) 366–373.
[5] J.W. Wang, Y.D. Li, Synthesis of single-crystalline nanobelts of ternary bismuth oxide bromide with different compositions, Chem. Commun. 232 (2003) 0–2321.
[6] J. Geng, W.H. Hou, Y.N. Lv, J.J. Zhu, H.Y. Chen, One-dimensional $BiPO_4$ nanorods and two-dimensional BiOCl lamellae: fast low-temperature sonochemical synthesis characterization, and growth mechanism, Inorg. Chem. 44 (2005) 8503–8509.
[7] Z.T. Deng, D. Chen, B. Peng, F.Q. Tang, From bulk metal Bi to two-dimensional well-crystallized BiOX (X = Cl, Br) micro- and nanostructures: synthesis and characterization, Cryst. Growth Des. 8 (2008) 2995–3003.
[8] X. Zhang, Z.H. Ai, F.L. Jia, L.Z. Zhang, Generalized one-pot synthesis, characterization, and photocatalytic activity of hierarchical BiOX (X = Cl, Br, I) nanoplate microspheres, J. Phys. Chem. C 112 (2008) 747–753.
[9] M.J. Earle, P.B. McCormac, K.R. Seddon, Diels–Alder reactions in ionic liquids. A safe recyclable alternative to lithium perchlorate–diethyl ether mixtures, Green Chem. 1 (1999) 23–25.
[10] D.J. Cole-Hamilton, Homogeneous catalysis-new approaches to catalyst separation, recovery, and recycling, Science 299 (2003) 1702–1706.
[11] F. Endres, M. Bukowski, R. Hempelmann, H. Natter, Electrodeposition of nanocrystalline metals and alloys from ionic liquids, Angew. Chem. Int. Ed. 42 (2003) 3428–3430.
[12] S. Dai, Y.H. Ju, H.J. Gao, J.S. Lin, S.J. Pennycook, C.E. Barnes, Preparation of silica aerogel using ionic liquids as solvents, Chem. Commun. 24 (2000) 3–244.
[13] Y. Wang, H. Yang, Synthesis of CoPt nanorods in ionic liquids, J. Am. Chem. Soc. 127 (2005) 5316–5317.
[14] D.B. Zhao, Z.F. Fei, W.H. Ang, P.J. Dyson, A strategy for the synthesis of transition-metal nanoparticles and their transfer between liquid phases, Small 2 (2006) 879–883.
[15] B.G. Trewyn, C.M. Whitman, V.S.Y. Lin, Morphological control of room-temperature ionic liquid templated mesoporous silica nanoparticles for controlled release of antibacterial agents, Nano Lett. 4 (2004) 2139–2143.
[16] M. Antonietti, D. Kuang, B. Smarsly, Y. Zhou, Ionic liquids for the convenient synthesis of functional nanoparticles and other inorganic nanostructures, Angew. Chem. Int. Ed. 43 (2004) 4988–4992.
[17] Y. Qin, Y. Song, N.J. Sun, N.N. Zhao, M.X. Li, L.M. Qi, Single-crystalline dendritic gold nanostructures with a three-fold symmetry, Chem. Mater. 20 (2008) 3965–3972.
[18] H.J. Ryu, L. Sanchez, H.A. Keul, A. Raj, M.R. Bockstaller, Imidazolium-based ionic liquids as efficient shape-regulating solvents for the synthesis of gold nanorods, Angew. Chem. Int. Ed. 47 (2008) 7639–7643.
[19] K.L. Ding, Z.J. Miao, Z.M. Liu, Z.F. Zhang, B.X. Han, G.M. An, S.D. Miao, Y. Xie, Facile synthesis of high quality TiO_2 nanocrystals in ionic liquid via a microwave-assisted process, J. Am. Chem. Soc. 129 (2007) 6362–6363.
[20] T. Nakashima, N. Kimizuka, Interfacial synthesis of hollow TiO_2 microspheres in ionic liquids, J. Am. Chem. Soc. 125 (2003) 6386–6387.
[21] Y. Zhou, M. Antonietti, Synthesis of very small TiO_2 nanocrystals in a room-temperature ionic liquid and their self-assembly toward mesoporous spherical aggregates, J. Am. Chem. Soc. 125 (2003) 14960–14961.
[22] L.X. Yang, Y.J. Zhu, W.W. Wang, H. Tong, M.L. Ruan, Synthesis and formation mechanism of nanoneedles and nanorods of manganese oxide octahedral molecular sieve using an ionic liquid, J. Phys. Chem. B 110 (2006) 6609–6614.
[23] J. Jiang, S.H. Yu, W.T. Yao, H. Ge, G.Z. Zhang, Morphogenesis and crystallization of Bi_2S_3 nanostructures by an ionic liquid-assisted templating route: synthesis, formation mechanism, and properties, Chem. Mater. 17 (2005) 6094–6100.
[24] K. Biswas, C.N.R. Rao, Use of ionic liquids in the synthesis of nanocrystals and nanorods of semiconducting metal chalcogenides, Chem. Eur. J. 13 (2007) 6123–6129.
[25] A.M. Dattelbaum, S.N. Baker, G.A. Baker, N-alkyl-N-methylpyrrolidinium salts as templates for hexagonally meso-ordered silicate thin films, Chem. Commun. 93 (2005) 9–941.
[26] G.S. Attard, J.C. Glyde, C.G. Goltner, Liquid-crystalline phases as templates for the synthesis of mesoporous silica, Nature 378 (1995) 366–368.
[27] Y. Zhou, M. Antonietti, Preparation of highly ordered monolithic super-microporous lamellar silica with a room-temperature ionic liquid as template via the nanocasting technique, Adv. Mater. 15 (2003) 1452–1455.
[28] B.G. Trewyn, C.M. Whitman, V.S. Lin, Morphological control of room-temperature ionic liquid templated mesoporous silica nanoparticles for controlled release of antibacterial agents, Nano Lett. 4 (2004) 2139–2143.
[29] B. Lee, H.M. Luo, C.Y. Yuan, J.S. Lin, S. Dai, Synthesis and characterization of organic–inorganic hybrid mesoporous silica materials with new templates, Chem. Commun. 24 (2004) 0–241.
[30] W.W. Wang, Y.J. Zhu, Microwave-assisted synthesis of cobalt oxalate nanorods and their thermal conversion to Co_3O_4 rods, Mater. Res. Bull. 40 (2005) 1929–1935.
[31] C. Zhang, J. Chen, Y.C. Zhou, D.Q. Li, Ionic liquid-based all-in-one synthesis and photoluminescence properties of lanthanide fluorides, J. Phys. Chem. C 122 (2008) 10083–10088.
[32] J.M. Du, Z.M. Liu, Z.H. Li, B.X. Han, Y. Huang, J.L. Zhang, Synthesis of mesoporous $SrCO_3$ spheres and hollow $CaCO_3$ spheres in room-temperature ionic liquid, Micropor. Mesopor. Mater. 83 (2005) 145–149.
[33] N. Recham, L. Dupont, M. Courty, K. Djellab, D. Larcher, M. Armand, J.M. Tarascon, Ionothermal synthesis of tailor-made $LiFePO_4$ powders for Li-ion battery applications, Chem. Mater. 21 (2009) 1096–1107.
[34] G. Bühler, C. Feldmann, Microwave-assisted synthesis of luminescent $LaPO_4$:Ce, Tb nanocrystals in ionic liquids, Angew. Chem. Int. Ed. 45 (2006) 4864–4867.
[35] J.S. Lee, X.Q. Wang, H.M. Luo, S. Dai, Fluidic carbon precursors for formation of functional carbon under ambient pressure based on ionic liquids, Adv. Mater. 22 (2010) 1004–1007.
[36] J.P. Paraknowitsch, J. Zhang, D.S. Su, A. Thomas, M. Antonietti, Ionic liquids as precursors for nitrogen-doped graphitic carbon, Adv. Mater. 22 (2010) 87–92.
[37] D.Q. Zhang, G.S. Li, X.F. Yang, J.C. Yu, A micrometer-size TiO_2 single-crystal photocatalyst with remarkable 80% level of reactive facets, Chem. Commun. 438 (2009) 1–4383.
[38] D.Q. Zhang, G.S. Li, H.B. Wang, K.M. Chan, J.C. Yu, Biocompatible anatase single-crystal photocatalysts with tunable percentage of reactive facets, Cryst. Growth Des. 10 (2010) 1130–1137.
[39] C.R. Chenthamarakshan, K. Rajeshwar, E.J. Wolfrum, Heterogeneous photocatalytic reduction of Cr (VI) in UV-irradiated titania suspensions: effect of protons ammonium ions, and other interfacial aspects, Langmuir 16 (2000) 2715–2721.
[40] M. Andersson, L. Osterlund, S. Ljungstrom, A. Palmqvist, J. Phys. Chem. B 106 (2002) 10674–10679.
[41] H. Weingärtner, Understanding ionic liquids at the molecular level: facts, problems, and controversies, Angew. Chem. Int. Ed. 47 (2008) 654–670.
[42] H. Cölfen, M. Antoniett, Mesocrystals: inorganic superstructures made by highly parallel crystallization and controlled alignment, Angew. Chem. Int. Ed. 44 (2005) 5576–5591.
[43] S. Wohlrab, N. Pinna, M. Antonietti, H. Cölfen, Polymer-induced alignment of DL-alanine nanocrystals to crystalline mesostructures, Chem. Eur. J. 11 (2005) 2903–2913.

[44] M. Niederberger, H. Cölfen, Oriented attachment and mesocrystals: non-classical crystallization mechanisms based on nanoparticle assembly, Phys. Chem. Chem. Phys. 8 (2006) 3271–3287.
[45] T.Y. Kim, W.J. Kim, S.H. Hong, J.E. Kim, K.S. Suh, Ionic-liquid-assisted formation of silver nanowires, Angew. Chem. Int. Ed. 48 (2009) 3806–3809.
[46] B. Cheng, Y. Le, W.Q. Cai, J.G. Yu, Synthesis of hierarchical $Ni(OH)_2$ and NiO nanosheets and their adsorption kinetics and isotherms to Congo red in water, J. Hazard. Mater. 185 (2011) 889–897.
[47] X.X. Yu, J.G. Yu, B. Cheng, M. Jaroniec, Synthesis of hierarchical flower-like AlOOH and TiO_2/AlOOH superstructures and their enhanced photocatalytic properties, J. Phys. Chem. C 113 (2009) 17527–17535.
[48] M.A. Shannon, P.W. Bohn, M. Elimelech, J.G. Georgiadis, B.J. Marinas, A.M. Mayes, Science and technology for water purification in the coming decades, Nature 452 (2008) 301–310.
[49] T.Y. Leung, C.Y. Chan, C. Hu, J.C. Yu, P.K. Wong, Photocatalytic disinfection of marine bacteria using fluorescent light, Water Res. 42 (2008) 4827–4837.
[50] J.C. Yu, W.K. Ho, J.G. Yu, H.Y. Yip, P.K. Wong, J.C. Zhao, Efficient visible-light-induced photocatalytic disinfection on sulfur-doped nanocrystalline titania, Environ. Sci. Technol. 39 (2005) 1175–1179.
[51] J.C. Yu, J.G. Yu, W.K. Ho, Z.T. Jiang, L.Z. Zhang, Effects of F^- doping on the photocatalytic activity and microstructures of nanocrystalline TiO_2 powders, Chem. Mater. 14 (2002) 3808–3816.